American Mineralogist, Volume 76, pages 1081–1091, 1991

Physics of aqueous phase evolution in plutonic environments

Philip A. Candela
Laboratory for Mineral Deposits Research, Department of Geology, University of Maryland, College Park, Maryland 20742, U.S.A.

Abstract

Many mineral deposits appear to have been formed by fluids of magmatic-hydrothermal origin. However, the means of egress of magmatic fluids and the focusing of these fluids into sites of alteration and mineralization are not well understood.

High Lewis numbers for H_2O imply that H_2O will accumulate within a marginal boundary layer or crystallization interval within magma chambers. Three cases are discussed: (1) Magmatic H_2O exsolution occurs at $\ll$20% crystallization (at high initial magmatic H_2O concentrations or low pressures), inducing the rise of plumes laden with bubbles ($\pm$ crystals). (2) Magmatic H_2O exsolution occurs later (at moderate initial magmatic H_2O concentrations or moderate pressures), and vapor bubbles, trapped in an immobile crust, form a spanning cluster at critical percolation through which the magmatic aqueous phase can advect. (3) Vapor exsolution occurs in an immobile crust but with lower initial H_2O concentrations or at higher pressure, so that the spanning cluster at critical percolation is not achieved and the magmatic aqueous phase is dispersed through the subsolidus cracking front.

The likelihood of plume rise (relative to the rise of individual bubbles) can be evaluated by calculating the characteristic rise time for individual bubbles relative to the characteristic rise time for bubble-laden plumes. For bubbles of $r \leq 1$ cm, plume rise is likely.

Percolation theory indicates that a spanning cluster of the aqueous phase on a simple three-dimensional lattice is attained when the aqueous phase achieves a volume fraction of $\Phi_v = 0.31$. Percolation is attained for initial magmatic H_2O concentrations $>1-2\%$ at 0.5 kbar and $>4-5\%$ at 2 kbar. For lower H_2O concentrations and higher pressures, vapor will be dispersed through a rather diffuse cracking front. This analysis suggests that orthomagmatic-hydrothermal fluids can be transported and focused to sites of mineral deposition near the apical regions of magma chambers by either bubble-plume rise or advection through spanning clusters of bubbles.

Introduction: vapor evolution in intrusive systems

The last few decades have seen many advances in chemical modeling of magmatic differentiation processes. More recently, a number of studies have focused on chemical modeling of magmatic aqueous phase exsolution. However, many of the chemical models of magmatic vapor evolution in ore-forming systems (Candela, 1986, 1989, 1990) ignore the physical constraints on the systems that are being modeled. Whereas significant progress has been made in understanding ore fluid chemistry in porphyry, skarn, and related systems, the means of egress of the magmatic fluids from crystallizing plutons and the mechanisms by which these ore fluids are focused in sites of mineralization are not well understood.

The importance of orthomagmatic-hydrothermal fluids in porphyry-type and skarn-type deposits has been debated for many years in the geological literature. Norton (1982) demonstrates convincingly that nonmagmatic H_2O can be focused in regions of mineralization, with magma bodies acting solely as heat engines. The volume of country rock from which ore metals can be leached by nonmagmatic fluids is obviously much larger than the volume of the associated pluton. Therefore, if the country rock is the source of ore substance, there is little problem accounting for the quantity of ore metals in the anomaly. That meteoric H_2O is important in the genesis of these deposits is not contested. Conversely, S isotope data, summarized by Ohmoto and Rye (1979), and hydrogen and oxygen isotope data (cf. Sheppard et al., 1971) suggest that a magmatic aqueous phase may also be active in ore formation. Further, Cl and Cu concentrations found in fluid inclusions from porphyry copper and related deposits (Reynolds and Beane, 1985; Scherkenbach et al., 1985) may easily be accounted for by the evolution of an aqueous phase from arc magmas (Candela and Holland, 1986; Candela, 1989). At the Henderson deposit, one of the most heavily studied porphyry deposits in the world, Carten et al. (1988) demonstrate very close links between intrusions and ore zones. Differences in the mass of ore, intensity of alteration, and density of veins can be directly correlated with primary igneous features in the associated

0003–004X/91/0708–1081$02.00

stocks. Additionally, Hannah and Stein (1985), in isotopic studies of the Climax group deposits, show convincingly that Pb and S were not derived from the country rock but from the ore-related plutons. The intrusive complexes associated with the Climax, Urad-Henderson, and Mount Emmons-Redwell porphyry Mo deposits were emplaced in very different host rocks: Precambrian felsic gneisses, amphibolites, and granulites at Climax; a younger Precambrian granite at Henderson; and Cretaceous shales and sandstone at Mount Emmons-Redwell. These variations in host rocks support the contention that country rocks at sites of stock emplacement played no significant chemical role in the mineralization process (Hannah and Stein, 1985).

Yet the hypothesis that orthomagmatic-hydrothermal processes play a dominant role in porphyry ore genesis remains problematic: it fails to account fully for the origin of at least some of the ore constituents in porphyry deposits. Quoting from Carten et al. (1988):

> The absence of high temperature veins and associated hydrothermal alteration in deep cores of stocks, the distribution of ore about the high levels of stocks, the orientation of veins about the apex of stocks . . . are suggestive of initially high concentrations of molybdenum and volatiles in the apex of a stock immediately prior to the onset of significant crystallization. . . . Assignment of molybdenum in the ore shell about the Seriate stock to the volume of solid occupied by the apex . . . yields concentration levels in the apical magma of approximately 13,000 ppm molybdenum.

Based on these and other observations, a number of fundamental questions may be raised with regard to the physics of magmatic aqueous phase evolution, such as: (1) Why do some plutons possess focused zones of intense mineralization, whereas others do not? and (2) How can large quantities of ore metals be brought to sites of ore deposition, given the orthomagmatic-hydrothermal paradigm, when only small cupolas are intimately associated with mineralization?

As a step toward answering these formidable questions, a general, preliminary physical model has been constructed to account for aqueous phase evolution from felsic magmas. The model, which is based on current physical models of magma chambers, suggests means by which magmatic ore fluids may be scavenged from rather large volumes of magma and delivered to sites of ore deposition, and it provides rationales for discriminating "productive" from "nonproductive" plutons. Eventually, more sophisticated physical models may be wedded to chemical models, such as those presented in Candela (1986), Candela and Holland (1986), and Candela (1989), to provide a comprehensive model for the evolution of aqueous fluids from epizonal plutons. Thus, this paper is a modest attempt to answer a portion of the question of why magmatic-hydrothermal mineralization occurs where it does.

The aims of this paper do not include a detailed discussion of how fracturing occurs in the apical regions of magma chambers. That cupolas and apical stocks are the foci of mineralization is not an issue. Clearly, in some cases, the magmatic aqueous phase is focused toward these structures (given a magmatic-hydrothermal paradigm). Knapp and Norton (1981) show that fracturing resulting from both magma pressure and thermal stress is initiated in the upper regions of a pluton. Buoyant forces resulting from the delivery of copious amounts of fluids to these zones ensure that repeated fracturing will occur in these regions (Norton and Cathles, 1973). This subject has been addressed in other works (cf. Knapp and Norton, 1981). Rather, the mechanisms by which the aqueous phase is brought to the upper regions of magma chambers are the objects of this study.

General crystallization models

The primary process in the crystallization of a magma body is the irreversible loss of heat to the surroundings. Heat passes out of the magma at the margins of the body, and crystallization is localized in these regions. With time, the solidus moves toward the interior of the magma chamber, defining a moving margin.

Langmuir (1989) refers to crystallization that occurs at the margins of a chamber as in situ and considers two limiting cases that are pertinent to the present endeavor. In Langmuir's first case, crystallization occurs at an interface between solid and liquid. The degree of crystallization as a function of distance varies as a steplike function near the interface. The evolved liquid is convected away from the rather sharp solid-liquid interface because of a (positive or negative) change in its density upon differentiation (Fig. 1). In Langmuir's second case, crystallization occurs at the margins in a crystallization interval of finite thickness, here defined as the region between 99 vol% and 1 vol% crystallization, consistent with Brandeis and Jaupart (1987) (Fig. 2). In this case, the evolved, residual melt within the crystallization interval is trapped in an immobile crust or mush (Marsh, 1988a, 1988b) and does not mix with the bulk melt.

The first case is similar to the model presented by McBirney et al. (1985) and Sparks et al. (1984) and is applicable to systems where crystals plate (nucleate) on the walls of a container and where rapid changes in melt density occur with crystallization. The difference between the density of the fractionated melt and the surrounding less-fractionated melt may lead to compositionally driven side wall convection, which can redistribute some of the differentiated melt to other parts of the chamber. The residuum may remix with the bulk melt or rise and form a compositionally stratified cap of differentiated magma at the top of the chamber.

The second case is a limiting case of a model presented for the Hawaiian lava lakes where magmatic differentiation is confined mostly to crusts of solid + liquid (± gas), which trap nearly all the fractionated liquid (Marsh, 1988a, 1988b). These systems cool mainly by conduction (Peck et al., 1977), with convection relegated to a rather minor role. Experimental simulation of these systems by

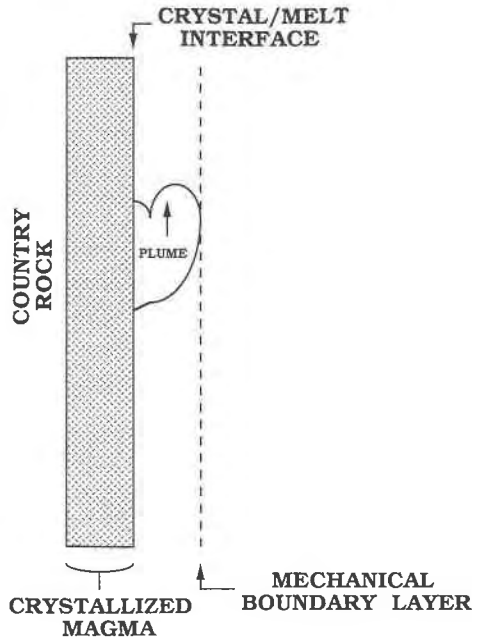

Fig. 1. A portion of a rising plume of bubble-laden melt along the margins of a magma chamber.

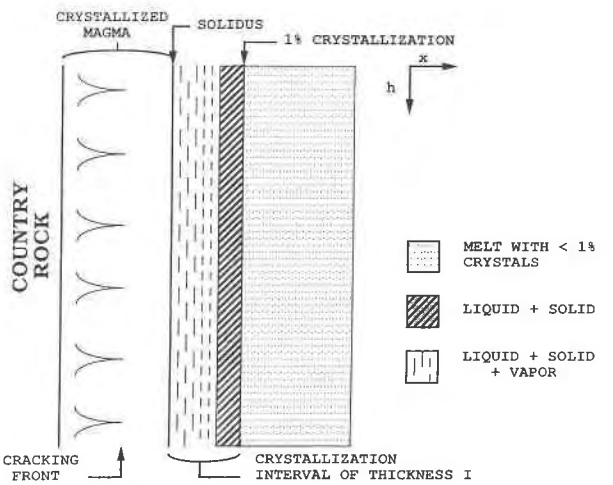

Fig. 2. Cross section of the margin of a magma chamber traversing (from left to right): country rock, cracked pluton, uncracked pluton, solidus, crystallization interval with liquid + solid ± aqueous fluid(s), and bulk melt. (See text for more details.)

Brandeis and Marsh (1989) supports this interpretation. Apparently, under some conditions, convection in subliquidus fluids is inhibited by crystallization. Langmuir (1989) suggests that the chemical trends found in some mafic systems can be explained by chemical processes that are intermediate between the extremes of cases 1 and 2, with the near-liquidus bulk magma mixing with more evolved, multiply saturated melts from the crystallization interval.

Now that the basic qualitative physical models for crystallization have been outlined, the modes of vapor saturation in these systems can be addressed. In the cooling of multicomponent liquids that are in homogeneous equilibrium, vapor saturation is the result of either a pressure decrease (first boiling) or the crystallization of anhydrous phases (second, or resurgent, boiling). In the case of second boiling, H_2O saturation will either occur ahead of the inward-advancing solidus for all x, t or occur late and in spatially segregated regions (e.g., the core of the plutonic complex), with H_2O back diffusing from the crystallization interval into the remaining body of the liquid.

The controls on the rate of crystallization need to be defined so that the behavior of H_2O in the region of crystallization can be determined. Given the importance of conduction relative to convection, summarized above, and the small thermal role attributed to convection for subliquidus systems (Brandeis and Marsh, 1989) and for systems not steadily heated from below (Marsh, 1988a, 1988b), a conductive model will be adopted here as the controlling factor in heat loss. Further, aside from transient effects where nucleation phenomena dominate, magmatic systems are probably attracted to a steady state characterized by a balance between crystal growth and heat loss to the country rocks (Brandeis et al., 1984). Therefore, for all but small times, the rate of advancement of the solidus is given by an expression (Jaeger, 1968) of the form

$$x = 0.28 \cdot t^{1/2} \tag{1a}$$

where x is the position of the solidus (crystallization proceeds in the positive x direction) in centimeters and t is time in seconds. (If x is recast in meters and t in years, the constant in Eq. 1a is approximately 16.) Equation 1a assumes a constant $\Delta T = 800$ °C (temperature of crystallization minus the temperature of the country rock far from the intrusion) at the contact and assumes a fixed melting point. However, Equation 1a does yield a first order estimate of the rate of advance of the crystallization front. For an order-of-magnitude estimate of the thickness of the crystallization interval, I, an equation has been extracted from Brandeis and Jaupart (1987) of the form

$$I = 0.93 \cdot t^{0.31} \tag{1b}$$

where I is in centimeters and t is in seconds. Equation 1b assumes a Stephan number (the ratio of the latent heat of crystallization to the heat capacity of the melt times a temperature scale for crystallization) equal to 0.55, and crystal growth rates and nucleation rates on the order of 10^{-10} cm/s and 10^{-3} cm^{-3}/s, respectively. These growth and nucleation rates are reasonable estimates for the interior of pluton systems (see Brandeis and Jaupart, 1987, for more details on growth and nucleation rates and background on Eq. 1b). In Table 1, the position of the solidus (x) and the interval thickness (I) are given as a function of time for a spherical chamber with a radius of 1 km

TABLE 1. Solidus position, thickness of crystallization interval, and fractional volume change as a function of time

x (meters)	l (cm)	$\Delta V^*/V \times 10^4$	t (s)
0.89	33	4.5	10^6
2.8	67	9.0	10^8
8.9	138	17	10^7
28	281	36	10^8
89	573	64	10^9
280	1171	81	10^{10}
885	23	3.3	10^{11}

Note: Solidus position, x ($x = 0$ is the original magma to country rock contact), thickness of crystallization interval, l, and fractional volume change of chamber resulting from vapor exsolution as a function of time, using Equations 1a, 1b, and 20, respectively.

(volume = 4.19 km^3). This hypothetical chamber crystallizes in approximately 10^{11} s ($\approx$3000 yr). The crystallization interval increases in thickness from a centimeter scale early on to tens of meters near the time of complete crystallization.

Given this basic cooling model, the Lewis number ($Le \equiv k/D_{H_2O}$) for H_2O (hereafter referred to simply as Le) can be calculated. Le indicates whether the rate of diffusion of H_2O is greater or smaller than the rate of heat diffusion, the main control on the rate of advance of the crystallization front into the magma. Either H_2O saturation is locally achieved (high Le) at the site of crystallization (boundary zone vapor saturation) or H_2O back diffuses into the rest melt (low Le). Given the range of H_2O diffusion coefficients in rhyolites (10^{-7} to 10^{-8} cm^2/s) and the thermal diffusivities found in rock systems (7×10^{-3} cm^2/s), the Lewis numbers are orders of magnitude above unity (log Le = 3.8–4.8). This indicates that the rate of diffusion of H_2O into the residual melt is insignificant relative to the rate of crystallization, and either H_2O accumulates in the crystallization interval or H_2O accumulates at the crystal-melt interface. The consequences of boundary zone vapor saturation will now be addressed in detail.

CASE 1: VAPOR SATURATION IN A BOUNDARY LAYER DURING SIDE WALL CRYSTALLIZATION

According to the models presented by McBirney et al. (1985) and Sparks et al. (1984), crystals are plated on the magma chamber side wall as crystallization proceeds. The H_2O concentration rises in the boundary layer until the aqueous-phase bubbles nucleate and grow. The mixture of bubbles and liquid will be referred to as a froth or a gas emulsion, depending upon the volume percent gas. According to Bikerman (1973), a foam has less than 10 vol% liquid, and the liquid phase is dominated by surface rather than by bulk properties. Froth is a rather ill-defined term that will be used here to denote the region between <10 vol% liquid (true foams) and >90 vol% liquid (gas emulsions). Here, the term froth will include gas emulsions. If crystals nucleate on the wall of the chamber (as in many crystallization experiments), then vapor bubbles will either rise separately or in plumes of vapor + liquid ± crystals. We can calculate the terminal velocity of rise of vapor bubbles by a Stokes-like formula or, more precisely, a Hadamard-Rybczynski (H-R) formula (Ramos, 1988). The H-R formulation accounts for motion in the boundary layer of the bubbles by employing a reduced drag coefficient, thus allowing for a more rapid rise of the vapor bubbles. Bubbles of hydrosaline fluid will rise less rapidly, resulting in an increase in their population in the melt relative to bubbles of vapor. In case 1, the bubbles may gain access to the upper reaches of the magma chamber by H-R bubble rise or by rise of a plume of bubbles and liquid.

From the H-R formula, the characteristic time for the rise of bubbles of radius r in a chamber of characteristic height h, containing a magma with a dynamic viscosity of μ_l, a density difference between melt and vapor = $\Delta\rho$, and an acceleration due to gravity, g, is given by

$$t_{\text{bubble}} = 3 \cdot \mu_l \cdot h / r^2 \cdot g \cdot \Delta\rho. \quad (2)$$

For h = 1 km, r = 1 cm, $\mu_l = 10^8$ poise, g = 980 cm^2/s, and $\Delta\rho$ = 2 g·cm^{-3}, a minimum bubble rise time of 1.5 $\times$ 10^{10} s is calculated. For a lower viscosity melt ($\mu = 10^5$ poise), the rise time is reduced to 1.53 $\times$ 10^7 s.

If the presence of crystals or bubbles in the medium surrounding any given bubble is taken into account, the calculated viscosity of the medium increases. The rheology of crystal- and bubble-fluid mixtures has been discussed by Marsh (1981), in part, in an attempt to explain Daly's dichotomy of basaltic extrusions vs. granitic intrusions. According to Marsh, basalts are rarely seen with more than about 55 vol% crystals. Smith (1979) suggests that this limit constrains the eruption of silicic ash flows to those that are less than half crystalline. Apparently, the magma is too viscous to erupt (or in general, too viscous to flow) if a critical crystallinity is exceeded. For granitic magma (sensu stricto), Marsh suggests that the critical locking point may be as low as 20 vol% crystals. Hildreth (1981) presented data that support this general proposition. Marsh and Maxey (1985) present an equation for the variation in the viscosity of magma as a function of the volume fraction of particles. Assuming that the viscosity rises steeply as the proportion of crystals + bubbles (N) reaches 20% by volume, their equation becomes

$$\mu_{\text{froth}} = \mu_l / \langle \exp 2.5 \cdot \{N/[1 - (N/0.2)]\} \rangle. \quad (3)$$

Therefore, as the proportion of bubbles increases, the rise time for bubbles of any given diameter will increase.

The characteristic time for vapor + liquid plume rise is calculated using the Stokes formula in a manner similar to that used by Marsh (1988b) to calculate the flow time for crystal plumes. In this model, vapor bubbles accumulate in a boundary layer. The thickness of this boundary layer will be given by the diffusion distance for H_2O on the time scale for plume rise: $\delta^2 \approx 4D_w \cdot t$. The resulting formula is then

$$t_{\text{plume}} = \sqrt{9 \cdot h \cdot \mu / 8 \cdot g \cdot \Phi_v \cdot \Delta\rho \cdot D_w} \quad (4)$$

where $\Phi_v \cdot \Delta\rho$ is the density contrast between the bubble-laden liquid and the bulk melt, and μ is the density of the

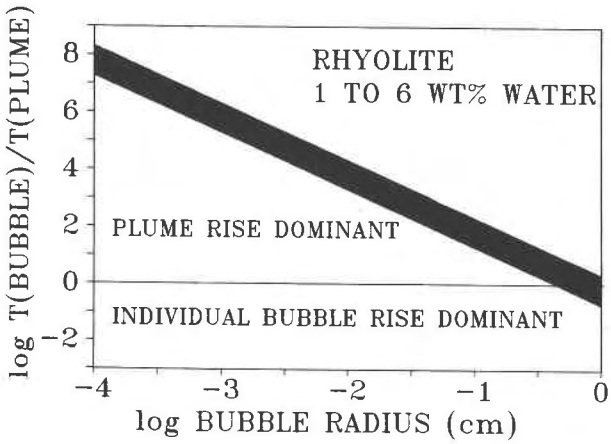

Fig. 3. Log of the ratio of the time scale of bubble rise to the time scale of plume rise vs. bubble diameter. The black band indicates solutions to Equation 4b for rhyolites with H_2O contents between 1 and 6 wt%. Note that plumes rise faster (i.e., have smaller characteristic rise times) for bubble radii less than 1 cm.

melt surrounding the plume. In the case of a "deep" epizonal felsic magma ($p \cong 2$ kbar, 6 wt% H_2O at saturation, depths on the order of 7–8 km), $\mu = 10^5$ poise (McBirney and Murase, 1971) and $D_{H_2O} = 10^{-7}$ cm^2/s (Delaney and Karsten, 1981). Characteristic times (t_{plume}) for the rise of a bubble-laden plume in a deep magma are on the order of 3.4×10^7 s (1 yr) or less. For a "shallow" magma, the lower H_2O concentrations result in higher viscosities and lower diffusivities, and plume rise times are on the order of 0.9 to 3.4×10^9 s (28–109 yr).

In the case of a deeper epizonal system, the plume rise time is on the same order as the rise time for large ($r \sim$ 1 cm) bubbles. However, most bubbles will have smaller radii and therefore much longer rise times. In Figure 3, the ratio of t_{bubble} to t_{plume}, obtained by dividing Equation 2 by Equation 4,

$$(t_{bubble}/t_{plume}) = (20/r^2)\cdot(\mu_l \cdot D_w \cdot \Phi_v)^{1/2} \qquad (4b)$$

is plotted vs. bubble radius (on a log-log plot) for Φ_v (within the plume) = 0.1. Over a large range of bubble radii, t_{plume} is much smaller than t_{bubble}, indicating that if vapor bubbles accumulate in a crystal-poor boundary layer, then the bubble-laden liquid is apt to rise to the top of the chamber. The density of H_2O vapor is reduced upon rise because of its small bulk modulus; therefore, the buoyancy of a plume is further enhanced by positive feedback. This process of bubble-laden plume flow may be a driving force for convection in some magma chambers. Common miarolitic cavities are probably the result of the decompression of vapor bubbles that were originally smaller than the crystals growing from the same melt. The expansion of the bubbles probably results from decompression during plume rise. Granitic melts lacking miarolitic cavities should not be interpreted as having been undersaturated with H_2O. Rather, those granites with miarolitic cavities may have crystallized under conditions where the initial H_2O concentration was within 80–90% of saturation. For most melts, this restricts the pressure during crystallization to approximately 1 kbar ($\approx$4 wt% H_2O at saturation), although melts with higher initial H_2O concentrations, such as those from muscovite-bearing sources, may possess miarolitic cavities at much greater depths.

This boundary layer model differs from other models (e.g., Sparks et al. 1984; Nilson et al., 1985) by explicitly considering the presence of vapor bubbles in promoting compositional side wall convection. One potentially significant complication associated with this analysis is the competition between the rate of rise of a plume and the rate of crystal nucleation and growth due to decompression and loss of vapor. This is similar to the problem of isothermal undercooling discussed by Westrich et al. (1988). Presumably, plume rise will terminate when the surrounding melt loses its fluidity. However, the systematics developed herein seem likely to be operative until the plume is adiabatically pressure quenched, as discussed by Norton and Knight (1977), producing a quench aplite or microgranite in the apical portions of the chamber.

Case 2: vapor saturation in a crystallization interval

As the leading edge of the crystallization interval advances into the magma after the nucleation incubation period, the percent crystallization at the wall steadily climbs. Crystallization progress is given by F, which varies from 1 (100% liquid) to 0 (100% solid). At some time, depending on the depth and the initial H_2O concentration in the melt, a critical fraction of liquid remaining (F) is reached at the wall such that vapor saturation is achieved. A new progress variable, Z (the vapor exsolution progress variable), is set equal to unity at the initiation of vapor exsolution; Z progresses toward zero as vapor is exsolved. As crystallization proceeds, the $Z = 1$ front advances inward behind the $F = 1$ front. Note that H_2O-saturated melt is confined to the crystallization interval (see Fig. 4). Even though the presence of vapor bubbles reduces the bulk density of the crystallization interval relative to its surroundings, and although there is no critical Raleigh number for convection in a horizontal density gradient, a few tens of percent (by volume) of bubbles plus crystals greatly reduce the probability of flow of the melt + vapor + crystal mixture because of the increased viscosity. In the limiting case of vapor saturation in a crystallization interval, vapor bubbles are probably trapped in an immobile crust. The aqueous fluid can only be removed from the sites of bubble nucleation through the establishment of a three-dimensional critical percolation network and advection of aqueous fluids through it or by means of the flow of fluid through a cracking front that is likely to form some 10–100 °C below the solidus.

On a three-dimensional, simple cubic lattice consisting of particles A and B (with number fractions $X_A < X_B$), critical percolation is said to occur, that is, a spanning

cluster of A is formed from one end of the lattice to another, when approximately 31% of the lattice points are occupied by A (Sur et al., 1976; Feder, 1988). This result was obtained by Monte Carlo simulations on a 50 × 50 × 50 grid and generalized using scaling laws. If the vapor-liquid-crystal region is modeled as a simple cubic lattice with the aqueous fluid as the potentially percolating phase, advection of the fluid upward may be considered possible when the volume fraction of the aqueous phase in the crystallization interval reaches approximately 0.31. The flux of H_2O at critical percolation may be low; however, as the volume fraction increases beyond the critical percolation threshold, the advective flux (driven by buoyancy and the positive pressure gradient produced by vapor exsolution, and allowed by the ability of the melt and the vapor to flow into the region vacated by advecting fluid) will increase rapidly (a type of gravitationally driven filter pressing of vapor).

Critical percolation begins at the wall and sweeps inward behind the zone of vapor bubble nucleation (see Fig. 4). It is followed by the solidus. The zone of percolation occurs between the solidus and a surface characterized by the critical value of the vapor exsolution progress variable (Z) at which percolation commences (Z_{CP}). For an idealized, hypothetical hemispherical magma chamber, this zone of percolation is a hemispherical shell that moves inward and thickens with time, as does the crystallization interval (Brandeis and Jaupart, 1987). The rate of increase of the volume fraction of vapor is significantly retarded as V_v/V_{sys} exceeds 0.31 because of the upward advection of the vapor from the system. This large volume change is, of course, not experienced by the whole magma chamber but only by the hemispherical shell of percolation, which is centimeters to meters thick.

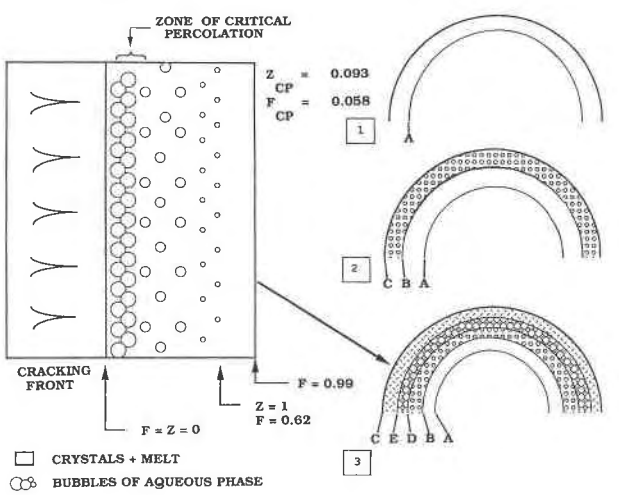

Fig. 4. Detailed, idealized illustration of the production of a spanning cluster of vapor bubbles at critical percolation. Initial H_2O concentration = 2.5%, H_2O saturation = 4%. Under these conditions $Z_{CP} = 0.093$ and $F_{CP} = 0.058$. Three stages in the formation of a crystallization interval upon intrusion are shown in the right portion of the figure: A is the leading edge of the crystallization interval, B is the leading edge of the zone of aqueous phase saturation, C is the magma to country rock contact, D is the leading edge of the zone of percolation, and E is the solidus.

Below, I present the derivation of the expression for Z_{CP}. In this derivation, the volume of liquid (V_l) and volume of crystals (V_{xl}) will be expressed as a function of the volume of vapor (V_v). The common factor V_v will then be removed from the right-hand side of the equation

$$V_{sys}(F) = V_v + V_l + V_{xl} \tag{5}$$

(which expresses the volume of the aqueous phase + melt + crystal system for any given value of F) to form an expression for $V_{sys}(F)/V_v$, the reciprocal of which is $\Phi_v \equiv V_v/V_{sys}(F)$, the volume fraction of vapor in the system at any time. Embarking on this derivation, let

$$F \equiv V_l/V_l^0. \tag{6}$$

Also, assuming a constant density for the liquid during differentiation, $F = M_l/M_l^0$. Modeling H_2O as a perfectly incompatible substance (the presence of a few percent hydrous minerals does not affect the substance of the argument), the critical F value at H_2O saturation is

$$F^s \equiv M_l^s/M_l^0 = V_l^s/V_l^0 = C_w^{l,0}/C_w^{l,s}. \tag{7}$$

The vapor exsolution progress variable, Z, is unity at vapor saturation and zero when $F = 0$ at the cessation of crystallization: $Z = (C_w^{l,s}/C_w^{l,0} \cdot F)$ or

$$F = Z \cdot F^s. \tag{8}$$

Because $V_{xl} \approx V_l^0 - V_l$,

$$V_{xl}/V_l^0 \approx 1 - F. \tag{9}$$

Combining Equations 6, 8, and 9 yields

$$V_l = V_{xl} \cdot [F^s Z/(1 - F^s Z)]. \tag{10}$$

An expression for V_{xl} may be obtained from the definition of the density of the melt at the commencement of vapor saturation combined with the volume form of Equation 7:

$$M_l^s = \rho_l \cdot F^s \cdot V_l^0. \tag{11}$$

Substituting Equation 8 into Equation 9 and combining the result with Equation 11 gives

$$M_l^s = \rho_l \cdot F^s \cdot V_{xl}/(1 - F^s Z). \tag{12}$$

Given the mass balance of expression $M_v = M_w^{l,s} - M_w^l$ and the definitions $Z \equiv M_w^l/M_w^{l,s}$ and $C_w^{l,s} \equiv M_w^{l,s}/M_l^s$,

$$M_v = (1 - Z) C_w^{l,s} \cdot M_l^s. \tag{13}$$

Combining Equations 12 and 13 to eliminate M_l^s and solving for V_{xl} results in the expression

$$V_{xl} = \frac{M_v \cdot (1 - F^s Z)}{(1 - Z) \cdot C_w^{l,s} \cdot \rho_l \cdot F^s}. \tag{14}$$

Substituting Equations 10 and 14 into the basic volume equation for the system (Eq. 5) and letting $M_v = \rho_l \cdot V_v$ yields

$$V_{sys}(F) = V_v + \frac{\rho_v \cdot V_v \cdot (1 - F^s Z)}{(1 - Z) \cdot C_w^{l,s} \cdot \rho_l \cdot F^s} \times \left[1 + \left(\frac{F^s Z}{(1 - F^s Z)}\right)\right]. \quad (15)$$

Simplifying Equation 15, substituting the identity from Equation 7 in the form $F^s = C_w^{l,0}/C_w^{l,s}$, and rearranging gives

$$\Phi_v = V_v/V_{sys} = \langle 1 + \{\rho_v/[\rho_l(1 - Z) \cdot C_w^{l,0}]\}\rangle^{-1}.$$

Letting $\Phi_v = 0.31$ from percolation theory yields a Z at critical percolation (Z_{CP}) given by

$$Z_{CP} = \left(1 - \frac{0.45 \cdot (\rho_v/\rho_l)}{C_w^{l,0}}\right). \quad (16)$$

Z_{CP} can be transformed into the critical F value, F_{CP}, (the critical value of the crystallization progress variable at percolation) by multiplying Equation 16 by F^s, yielding

$$F_{CP} = [C_w^{l,0} - 0.45(\rho_v/\rho_l)]/C_w^{l,s}. \quad (17)$$

The condition of $F_{CP} = 0$ is a limiting case of Equation 17 that indicates the onset of critical percolation at 100% crystallization. Setting $F_{CP} = 0$ in Equation 17 yields

$$\left(\frac{C_w^{l,0}}{C_w^{l,s}}\right)_{F_{CP}=0} = \frac{0.45 \cdot \rho_v}{C_w^{l,s} \cdot \rho_l}. \quad (18)$$

The left-hand side of Equation 18 indicates the minimum ratio of the initial H_2O concentration in the melt to the H_2O concentration at saturation, for a given total pressure, at which a spanning cluster of vapor bubbles will form. Spanning clusters will form in the crystallization intervals of all wetter magmas (higher $C_w^{l,0}$) at the same total pressure. Conversely, drier magmas at the same total pressure will not achieve a state of critical percolation. With increasing pressure, the density of the aqueous phase increases more rapidly than the solubility of H_2O in the melt, resulting in an increase in the minimum $C_w^{l,0}/C_w^{l,s}$ for which a spanning cluster of vapor bubbles will form within a crystallization interval (see Fig. 5). At magma pressures equal to or greater than approximately 1.7 kbar, critical percolation is not achieved at any initial H_2O concentration. If F_{CP} lies between 1 and 0, then significant amounts of fluid can be removed and concentrated before the solidus isotherm sweeps through the system. If F_{CP} is negative, critical percolation is never achieved, and H_2O is probably pumped out of the system through the cracking front; this is discussed in the next section of this paper.

The approach taken here, essentially a "modified mass balance approach" coupled with a phenomenological physical model rooted in elementary percolation theory, obviously neglects some effects, such as the spatial distribution of bubbles on a small scale and nucleation control of bubble size distribution. However, these parameters are likely to affect the particular values of F_{CP} or Z_{CP}

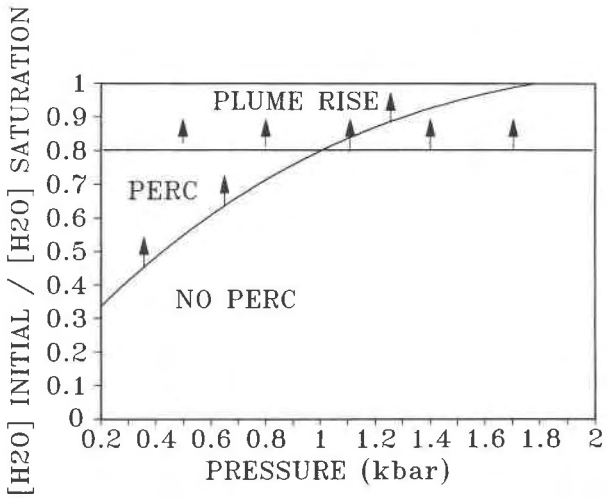

Fig. 5. The curved line indicates, for a given pressure, the minimum ratio of the initial magmatic H_2O concentration to the magmatic H_2O concentration at saturation [(H_2O initial)/(H_2O saturation)] at which a spanning cluster of vapor bubbles will allow the upward advection of magmatic H_2O. Further, in a rhyolitic system, bubble-laden plume rise is expected for values of the (H_2O initial)/(H_2O saturation) = 0.8. Arrows indicate regions of graph favoring large-scale upward transport of the magmatic aqueous phase.

or the specific relationship between permeability and porosity of the crystallization interval, rather than the conceptual features of the physical model.

Given this concept of critical percolation, advection of the aqueous phase occurs as porous media flow through the spanning cluster of vapor bubbles. An illustrative calculation can be performed by using data on the relationship of permeability to porosity for obsidian reported in Eichelberger et al. (1986). At a porosity of 37%, the obsidian exhibited a permeability on the order of $k = 10^{-12}$ cm^2, the lowest permeability measured in their study. At higher porosities (up to 74%), the permeability climbed to almost $k = 10^{-8}$ cm^2. Therefore, calculations from this study provide a minimum estimate for the fluid flux of an upwardly aqueous phase. The estimate is most accurate for porosities close to the Φ_v of the original spanning cluster. Given kinematic viscosities for the aqueous phase on the order of 10^{-3} cm^2/s at 800 °C and 1 kbar (Norton and Knight, 1977), a Darcy fluid flux can be calculated from the equation $Q = (k/\nu) \cdot (\Delta p/h)$. After the spanning cluster of vapor bubbles is achieved, the pressure at any point in the column of vapor will be less than that in the adjacent melt by a factor of $\Delta p = g \cdot h \cdot \Delta\rho$, where g = the acceleration due to gravity, h = characteristic height of the magma chamber, and $\Delta\rho \approx 2$ g·cm^{-3} is the difference in density between the melt and vapor. In this case,

$$Q = (k/\nu) \cdot g \cdot \Delta\rho. \quad (19)$$

This calculation yields a minimum value of $Q = 10^{-6}$ g·cm^{-2}/s, which is comparable to the largest fluid fluxes

calculated in the convective systems surrounding magma-hydrothermal systems (Norton, 1982). Obviously, these fluxes are sufficient to deliver significant amounts of fluid to upper portions of a magma chamber.

At this point, the effect of the chlorinity of the magma and the associated aqueous phase may be addressed. When the magmatic aqueous fluid composition is in the two-phase region of the system NaCl-H_2O for pressures below approximately 1.4 kbar at 800 °C (Bodnar et al., 1985), some fraction of hydrosaline fluid (with a density on the order of unity) will be present. As a result of its lower density, one might expect the vapor to be fractionated relative to the hydrosaline fluid, although both will rise to the top of the chamber. The vapor may, however, rise faster. Whereas the hydrosaline fluid is buoyant within the confines of the magmatic system ($\rho_{melt} > \rho_{hydrosaline\ fluid}$), it is not buoyant within the surrounding geothermal system. For example, given that cold ground H_2O has a density on the order of unity, vapor-saturated hydrosaline liquids with salinities greater than 50% NaCl (at 500 bars pressure and temperatures greater than approximately 550 °C) will not be buoyant within the hydrothermal system. (The interested reader is referred to Henley and McNabb, 1978, especially Fig. 4 therein, for further considerations of this type.) The hydrosaline fluid will tend to pond in the crystal mush near the roof, possibly creating a stable, stratified deep brine zone (cf. Henley and McNabb, 1978). This may account for the trapping of hydrosaline fluids as opposed to vapor in inclusions in magmatic minerals in the upper reaches of plutonic complexes (Frezzotti and Ghezzo, 1989).

Although the crystallizing magma experiences volume increases on the order of 45% [the relative volume change, $\Delta V/V \equiv (V_v - V_0)/V_0$, is equal to 0.45 when $\Phi_v \equiv V_v/(V_v + V_{xl} + V_{melt})$ is equal to 0.31], the volume of the crystallization interval is rather restricted (see Table 1). The total volume increase of the magma chamber is therefore rather modest. The value of $\Delta V/V$ can be calculated by considering vapor evolution to occur in a spherical shell bounded by the solidus (at x) and the leading edge of the crystallization interval (at $x + I$) at any time such that

$$\Delta V/V|_{max} = 0.45 \cdot [(1 - x)^3 - (1 - x - I)^3] \quad (20)$$

for a magma chamber with a radius of 1 km. The $\Delta V/V$ is tabulated in Table 1.

It is not the purpose of this paper to provide a model for the fracturing of plutons; however, the crystallization and vapor saturation model presented here does allow for the fracturing of a magma chamber by magma pressure, and this will be discussed briefly. Given tensile strengths of roof rocks on the order of 100 bars (cf. Suppe, 1985), a Mohr circle analysis with a combination Griffith-Coulomb failure envelope suggests that pure tensional failure is indicated for magma overpressures (ΔP) on the same order as the tensile strength, with a Mohr circle radius of approximately ΔP. A crude approximation of the overpressure produced in a magma chamber, neglecting shear deformation of the roof and neglecting volume changes resulting from crystallization (aside from second boiling), can be obtained using the coefficient for compressibility of the magma. Taking $\beta \cong 10^{-5}$ bars^{-1} and $\Delta P \approx 10^2$ bars for pure tensile failure yields $\Delta V/V \approx \Delta P \cdot \beta \approx 10^{-3}$, suggesting that failure of the chamber occurs with a whole-chamber fractional volume increase on the order of 0.1. This result is in good agreement with the more sophisticated analysis of Tait et al. (1989), who suggest that failure occurs with fractional changes in volume of $0.2 - 0.8 \times 10^{-3}$. Inspection of Table 1 suggests that failure occurs early (after about 1 yr) and continues throughout much of the crystallization history of the magma chamber. The whole-chamber volume changes are on the same order as those required to fracture the roof zone of the chamber.

Creation of the magmatic vapor-disperse system: the lack of critical percolation

According to Knapp and Norton (1981), thermal stresses generated by the cooling of a pluton cause rock failure by brittle fracture. Fracture permeability develops adjacent to the magma-rock interface under conditions where the igneous rock fails. Norton and Taylor (1979) modeled fracturing in the Skaergaard system by assuming that the pluton fractured when the temperature decreased to 50 °C below the solidus. For porphyry copper systems, Norton (1982) has used a figure of 100 °C below the solidus for magma-induced fracturing in already-crystallized portions of the pluton. This latter figure is supported by stress-strain calculations for the no-strain case; with reasonable values for Poisson's ratio, the elastic constant, and thermal expansion, ΔT on the order of 100 °C yields effective stresses on the order of 10^2 bars, which is on the same order as the tensile strength of many rocks. In cases where the critical Z of percolation is outside the domain of the Z variable in a real system (i.e., negative values of Z_{CP}), the accumulated aqueous phase will remain in pores, vesicles, or miarolitic cavities until provided egress through the cracking front and entrained in the meteoric H_2O flow. Even though these packets of fluid may advect upward toward the zone of mineralization, the fluid experiences a rather rapid decrease in temperature upon rise and may be diluted by adjacent nonmagmatic fluids (cf. Norton and Knight, 1977). This is clearly different from the percolation case wherein fluid advects through the melt under quasi-isothermal conditions to a localized, albeit downward migrating region. Because of the accelerated cooling and dilution of the magmatic fluids upon transport in the absence of critical percolation, this mechanism is likely to result in scattered shows of mineralization rather than centralized zones of intense alteration and mineral deposition. This will be termed a magmatic vapor–disperse system because egress of the fluid through the cracking front results in a much more heavily dispersed zone of metasomatism from magmatic H_2O.

Discussion

This paper has described two possible processes by which magmatic aqueous fluids may be delivered to the upper regions of felsic magma chambers. Both mechanisms, plume rise and critical percolation, may be operative in nature depending on the conditions prevailing upon crystallization. Further, a synthesis will be presented that unites the two models presented in this paper (i.e., the formation of a crystallization interval with melt "locked in" vs. side wall compositional convection) through the process of vapor exsolution. The critical factor determining the behavior of a given system, within the framework of the models presented in this paper, is the rate of change of the density of the crystal-melt-vapor system as crystallization proceeds. This rate is controlled by the timing of vapor evolution (which, in turn, is controlled by $C_w^{l,0}/C_w^{l,s}$) and by the density of the aqueous phase (which, in turn, is controlled dominantly by pressure and to a lesser extent by temperature). For magmas with high values of $C_w^{l,0}/C_w^{l,s}$ (note that the maximum value for this ratio is unity under equilibrium conditions), vapor saturation occurs early (at high F values), and significant buoyancy is achieved at relatively low viscosity (crystallinity). In this case, plumes may rise from a subvertical border zone. Given that the probability of eruption of a granitic melt is significantly decreased for crystallization greater than 20%, vapor evolution probably must occur at F values greater than 0.8 for this mechanism to be operative. This effect is obviously enhanced at lower pressures because of the effect of reduced pressure on density and, hence, buoyancy. Here, side wall crystallization is seen as a special case of the crystallization interval-percolation model, where $C_w^{l,0}$ is sufficiently high and pressure sufficiently low that the presence of bubbles at low crystallinity on the inner (leading) edge of the interval induces plume rise. This might result if, for example, a magma with few crystals and 3 wt% H_2O intruded to a depth of approximately 1.9 km (equilibrium H_2O solubility equal to approximately 3 wt%). Under these conditions, a few percent crystallization would induce vapor bubble formation and plume rise. If, however, this same magma were to intrude to a depth of 3.5 to 4 km, then the first bubbles may not form until approximately 25% crystallization occurred. The high viscosities realized in felsic systems with greater than 20% crystals (Marsh, 1981) might preclude plume rise under these conditions. However, critical percolation is achieved at $F = 0.2$ (i.e., after 80% crystallization); in this somewhat deeper case, the delivery of vapor to the apical portions of a chamber would be by advection through a spanning cluster of vapor bubbles. This percolation interval sweeps inward and downward with time through the chamber. If this same initial magma were to crystallize at a greater depth (e.g., greater than 7–8 km), then both plume rise and critical percolation would be precluded. The only means of egress available for the magmatic volatile phase(s) under supersolidus conditions would be by a highly tortuous rise of individual vapor bubbles through a crystal-choked immobile crust within the crystallization interval. In this case, bubble rise is likely to experience a much greater drag force than that accounted for by either Stokes or Hadamard-Rybczynski drag coefficients. Most likely, this would result in a vapor-disperse system with little focusing of the flow of magmatic H_2O.

Therefore, boundary-layer second boiling in systems with high *Le* numbers at a variety of $C_w^{l,0}$ and pressures spans the range between systems allowing side wall (plume) fractionation at high $C_w^{l,0}$ and low pressure, on one hand, and those resulting in low-mobility rest melt $\pm$ upwardly percolating vapor at lower $C_w^{l,0}$ and high pressures, on the other hand. The observable characteristics of these cases will reflect the mode of vapor transport. In the case of plume rise, the quenching of the plumes will result in aplites, miarolitic granites, and porphyries with fine-grained groundmass. Zones of intense alteration and mineralization may surround these bodies. In the case of advection through a spanning cluster, hydrothermal alteration may be centered on the apical region of the pluton, but strong textural variation is not expected. In the case of the vapor-disperse system, alteration and mineralization will be dispersed throughout a large volume. When present, concentrated zones will be small in volume and not necessarily concentrated in apical regions.

The discussion in this paper is predicated on the condition that H_2O is characterized by large *Le* numbers in magmatic systems. There may, however, be magmatic systems (still not well studied) that possess relatively low viscosities and high diffusivities. London (1986) and London et al. (1989) have discussed the effects of increasing Li, B, P, F, and H on crystallization and vapor exsolution in pegmatitic systems. In melts with anomalously large concentrations of these elements, it is possible to generate melts with low viscosity, high diffusivity, and greatly enhanced H_2O solubility. This combination of lowered *Le* numbers and elevated H_2O solubilities could result in a significant delay in vapor saturation in these magmas, and vapor saturation might occur only in restricted portions of an intrusion. The style and texture of crystallization and the style of vapor evolution would be very different in such systems. London et al. (1989) have pointed out that the increase of the structure-breaking components Li, B, P, F, and H in felsic systems may lead to a reduction in nucleation rates of feldspar as the short-range structure of the melt deviates significantly from tectosilicate-like units. The reduction in nucleation rate leads to the production of pegmatitic textures. These systems may evolve a vapor only from restricted portions of the magma chamber.

Conclusions

Simple physical analysis of the crystallization of felsic magmas in light of recent studies of magma dynamics

suggests that the achievement of critical percolation within a crystallization interval is possible if the initial H_2O concentration of the magma is above a minimum value for a given pressure (Fig. 5) and if the system is at a pressure of less than 2 kbar. Fracturing by second boiling is consistent with this model, and aqueous fluids will advect to the apical portions of magmas without experiencing significant cooling or mixing with meteoric or other H_2O. In systems with high enough H_2O concentrations for a given intrusion pressure or in cases where crystal nucleation occurs dominantly along the walls of the chamber, plumes of bubble-laden melt may raft to the top of the magma chamber. These buoyantly rising plumes may erupt, yielding permeable froths (Eichelberger et al., 1986), or may form apophyses, dikes, or lift cupolas by virtue of their buoyancy. These models account for the delivery of magmatic aqueous fluid from large portions of magma chambers to the upper portions where mineralized zones are formed. This may explain how large amounts of magmatic vapor, charged with mineralizing agents such as Mo or Cu are focused into small regions, yielding large concentrations of ore metals that appear to be genetically related to small apical stocks, such as at the Henderson mine and related deposits. Therefore, systems that are capable of delivering large volumes of vapor to apical regions by plume flow or advection through spanning clusters possess a greater probability of developing into productive systems. Plumes rising to the top of a chamber may be pressure quenched, resulting in the crystallization of the vapor + melt mixture with time. The final product might be an aplite (London et al., 1989) consisting of an intimate mixture of igneous material (e.g., quartz and feldspar) and hydrothermal material (e.g., molybdenite), as is found in the upper regions of a number of silicic plutons (Öhlander, 1985). Some of these occurrences exhibit little alteration, as if only a small degree of cooling in the presence of aqueous fluids occurred before the aqueous phase was driven from the pluton. However, the molybdenite in these systems has precipitated at a high enough temperature to result in its incorporation in the aplitic granites. This is consistent with the high-precipitation temperatures found for molybdenite in volcanic gases (Bernard et al., 1990).

In systems that are relatively dry or deep and achieve neither critical percolation nor plume rise, the magmatic aqueous phase is apt to be released from the pluton in a more dispersed state, resulting in diffuse zones of metasomatism and mineralization. Disseminated molybdenite (Whalen, 1980) and scheelite or wolframite probably mark the incipient cooling and dilution of dispersed magmatic fluid and may characterize, at least in some cases, the nonproductive system.

Acknowledgments

Discussions over the last few years with Chip (C.E.) Lesher and Frank Spera inspired me to write this paper. Steve Lynton, Phil Piccoli, and Tom Williams are thanked for later discussions. A lengthy discussion with Bruce Marsh in December 1988 at the University of Maryland concerning crystallization, probability, and rheology was enlightening. Further comments by Steve Lynton, Dennis Bird, and an anonymous reviewer have greatly improved the manuscript. Special thanks to Barbara Lee for help with the figures. Mary Ostrowski and A. Ledbetter are thanked for providing additional inspiration. Of course, all errors in this paper are the responsibility of the author. The support of NSF grants EAR-8706198 and EAR-9004154 and the Magma Energy Project of DOE is gratefully acknowledged.

References cited

Bernard, A., Symonds, R.B., and Rose, W.I., Jr. (1990) Volatile transport and deposition of Mo, W and Re in high temperature magmatic fluids. Applied Geochemistry, 5, 317–326.

Bikerman, J.J. (1973) Foams, 337 p. Springer-Verlag, New York.

Bodnar, R.J., Burnham, C.W., and Sterner, S.M. (1985) Synthetic fluid inclusions in natural quartz. III. Determination of phase equilibrium properties in the system H_2O-NaCl to 1000 °C and 1500 bars. Geochimica et Cosmochimica Acta, 49, 1861–1874.

Brandeis, G., and Jaupart, C. (1987) Crystal sizes in intrusions of different dimensions: Constraints on the cooling regime and the crystallization kinetics. In B.O. Mysen, Ed., Magmatic processes: Physiochemical principles, p. 307–318. The Geochemical Society, New York.

Brandeis, G., and Marsh, B.D. (1989) The convective liquidus in a solidifying magma chamber: A fluid dynamic investigation. Nature, 339, 613–616.

Brandeis, G., Jaupart, C., and Allegre, C.J. (1984) Nucleation, crystal growth and the thermal regime of cooling magmas. Journal of Geophysical Research, 89, 10161–10177.

Candela, P.A. (1986) Generalized mathematical models for the fractional evolution of vapor from magmas in terrestrial planetary crusts. Advances in physical geochemistry, vol. 6; Chemistry and physics of the terrestrial planets, p. 362–396. Springer-Verlag, New York.

——— (1989) Magmatic ore-forming fluids: Thermodynamic and mass transfer calculations of metal concentrations. In Society of Economic Geologists Reviews in Economic Geology, 4, 223–233.

——— (1990) Theoretical constraints on the chemistry of the magmatic aqueous phase. Geological Society of America Special Paper, 246, 11–20.

Candela, P.A., and Holland, H.D. (1986) A mass transfer model for copper and molybdenum in magmatic hydrothermal systems: The origin of porphyry-type ore deposits. Economic Geology, 81, 1–19.

Carten, R.D., Geraghty, E.P., Walker, B.M., and Shannon, J.R. (1988) Cyclic development of igneous features and their relationship to high-temperature hydrothermal features in the Henderson porphyry molybdenum deposit, Colorado. Economic Geology, 83, 266–296.

Delaney, J.R., and Karsten, J.L. (1981) Ion microprobe studies of water in silicate melts: Concentration-dependent diffusion in obsidian. Earth and Planetary Science Letters, 52, 191–202.

Eichelberger, J.C., Carrigan, C.R., Westrich, H.R., and Price, R.H. (1986) Non-explosive silicic volcanism. Nature, 323, 598–602.

Feder, J. (1988) Fractals (1st edition), 283 p. Plenum Press, New York.

Frezzotti, M.L., and Ghezzo, C. (1989) Fluid phase evolution in the M. Genis leucogranitic intrusion (SE Sardinia, Italy). IAVCEI Conference Abstracts, 98.

Hannah, J.L., and Stein, H.J. (1985) Oxygen isotope compositions of selected Laramide-Tertiary granitoid stocks in the Colorado Mineral Belt and their bearing on the origin of Climax-type granite-molybdenum systems. Contributions to Mineralogy and Petrology, 93, 347–358.

Henley, R.W., and McNabb, A. (1978) Magmatic vapor plumes and ground-water interaction in porphyry copper emplacement. Economic Geology, 73, 1–20.

Hildreth, W. (1981) Gradients in silicic magma chambers: Implications for lithospheric magmatism. Journal of Geophysical Research, 86, 10153–10192.

Jaeger, J.C. (1968) Cooling and solidification of igneous rocks: In H.H. Hess and A. Poldervaart, Eds., Basalts, p. 503–536. Interscience Publishers, New York.

Knapp, R.B., and Norton, D. (1981) Preliminary numerical analysis of

processes related to magma crystallization and stress evolution in cooling pluton environments. American Journal of Science, 281, 35–68.
Langmuir, C.H. (1989) Geochemical consequences of *in situ* crystallization. Nature, 340, 199–205.
London, D. (1986) Magmatic-hydrothermal transition in the Tanco rare-element pegmatite: Evidence from fluid inclusions and phase equilibrium experiments. American Mineralogist, 71, 376–395.
London, D., Morgan, G.B., VI, and Hervig, R.L. (1989) Vapor-undersaturated experiments with Macusani glass + H_2O at 200 MPa and the internal differentiation of granitic pegmatites. Contributions to Mineralogy and Petrology, 102, 1–17.
Marsh, B.D. (1981) On the crystallinity, probability of occurrence, and rheology of lava and magma. Contributions to Mineralogy and Petrology, 78, 85–98.
——— (1988a) Causes of magmatic diversity. Nature, 333, 97.
——— (1988b) Crystal capture, sorting, and retention in convecting magma. Geological Society of America Bulletin, 100, 1720–1737.
Marsh, B.D., and Maxey, M.R. (1985) On the distribution and separation of crystals in convecting magma. Journal of Volcanology and Geothermal Research, 24, 95–150.
McBirney, A.R., Baker, B.H., and Nilson, R.H. (1985) Liquid fractionation. Part 1: Basic principles and experimental simulations. Journal of Volcanology and Geothermal Research, 24, 1–24.
Nilson, R.H., McBirney, A.R., and Baker, B.H. (1985) Liquid fractionation. Part II: Fluid dynamics and qualitative implications for magmatic systems. Journal of Volcanology and Geothermal Research, 24, 25–54.
Norton, D.L. (1982) Fluid and heat transport phenomena typical of copper-bearing pluton environments. In S.R. Titley, Ed., Advances in geology of porphyry copper deposits, p. 59–72. University of Arizona Press, Tucson, Arizona.
Norton, D.L., and Cathles, L.M. (1973) Brecciapipes—Products of exsolved vapor from magmas. Economic Geology, 68, 540–546.
Norton, D.L., and Knight, J. (1977) Transport phenomena in hydrothermal systems: Cooling plutons. American Journal of Science, 277, 937–981.
Norton, D., and Taylor, H.P., Jr. (1979) Quantitative simulation of the hydrothermal systems of crystallizing magmas on the basis of transport theory and oxygen isotope data: An analysis of the Skaergaard intrusion. Journal of Petrology, 20, 421–486.
Öhlander, B. (1985) Geochemistry of Proterozoic molybdenite mineralized aplites in northern Sweden. Mineralium Deposita, 20, 241–248.
Ohmoto, H., and Rye, R.O. (1979) Isotopes of sulfur and carbon. In H.L. Barnes, Ed., Geochemistry of hydrothermal ore deposits, p. 509–567. Wiley Interscience, New York.
Peck, D.L., Hamilton, M.S., and Shaw, H.R. (1977) Numerical analysis of lava lake cooling models: Part II. Application to Alae Lava Lake, Hawaii. American Journal of Science, 277, 415–437.
Ramos, J.I. (1988) Multicomponent gas bubbles II. Bubble dynamics. Journal of Non-Equilibrium Thermodynamics, 13, 107–131.
Reynolds, T.J., and Beane, R.E. (1985) Evolution of hydrothermal fluid characteristics at the Santa Rita, New Mexico, porphyry copper deposit. Economic Geology, 80, 1328–1347.
Scherkenbach, D.A., Sawkins, F.J., and Seyfried, W.E., Jr. (1985) Geologic, fluid inclusion, and geochemical studies of the mineralized breccias at Cumobabi, Sonora, Mexico. Economic Geology, 80, 1566–1592.
Sheppard, S.M.F., Nielsen, R.L., and Taylor, H.P., Jr. (1971) Hydrogen and oxygen isotope ratios in minerals from porphyry copper deposits. Economic Geology, 66, 515–542.
Smith, R.L. (1979) Ash flow magmatism. Geological Society of America Special Paper 180, 5–27.
Sparks, R.S.J., Huppert, H.E., and Turner, J.S. (1984) The fluid dynamics of evolving magma chambers. Royal Society of London Philosophical Transactions, A310, 511–534.
Suppe, J. (1985) Principles of structural geology (1st ed.), 537 p. Prentice-Hall, Princeton, New Jersey.
Sur, A., Lebowitz, J.L., Marro, J., Kalos, M.H., and Kirkpatrick, S. (1976) Monte Carlo studies of percolation phenomena for a simple cubic lattice. Journal of Statistical Physics, 15, 345–353.
Tait, S., Jaupart, C., and Vergniolle, S. (1989) Pressure, gas content and eruption periodicity of a shallow, crystallizing magma chamber. Earth and Planetary Science Letters, 92, 107–123.
Westrich, H.R., Stockman, H.W., and Eichelberger, J.C. (1988) Degassing of rhyolitic magma during ascent and emplacement. Journal of Geophysical Research, 93, 6503–6511.
Whalen, J.B. (1980) Geology and geochemistry of the molybdenite showings of the Ackley City batholith, southeast Newfoundland. Canadian Journal of Earth Science, 17, 1246–1258.

Manuscript received October 16, 1989
Manuscript accepted April 15, 1991

Appendix 1. Symbols

C_i^ϕ = concentration of i in phase ϕ (in weight fraction)
D = diffusion coefficient
F = crystallization progress variable
g = acceleration due to gravity
h = magma chamber height, measured from the top down
I = thickness of the crystallization interval
k = coefficient of thermal diffusivity
k = permeability
l = (subscript or superscript) liquid
Le = Lewis number
M_i = mass of phase i
0 = (subscript or superscript) value of variable in initial melt
P = pressure
Q = Darcy fluid flux
r = radius
s = (superscript) value of variable at water saturation
sys = (subscript) system
t = time in seconds (s) or years (yr)
V_i = volume of phase i
v = (subscript) vapor
w = (subscript) water
x = position of the solidus relative to the initial contact
xl = (subscript) crystal
Z = vapor exsolution progress variable
Z_{CP} = Z at critical percolation
β = coefficient of compressibility
δ = thickness of the rising boundary layer
μ = dynamic viscosity
Φ_i = volume fraction of phase i
ρ = density